Computational Design and Initial Corrosion Assessment of a Series of Non-Equimolar High Entropy Alloys

Pin Lu [a,1] , James E. Saal [a], Gregory B. Olson [a], Tianshu Li [b], Sarita Sahu [b], Orion J. Swanson [b], G. S. Frankel [b], Angela Y. Gerard [c], John R. Scully [c]

[a] *QuesTek Innovations LLC, 1820 Ridge Avenue, Evanston, IL 60201, USA*

[b] *Fontana Corrosion Center, The Ohio State University, Columbus, OH 43210, USA*

[c] *Center for Electrochemical Science and Engineering, University of Virginia, Charlottesville, VA 22904, USA*

Abstract

The integrated computational materials engineering approach has been employed to design a series of four single-phase non-equimolar high entropy alloys (HEAs) with systematically varied compositions ($Ni_{38}Fe_{20}Cr_xMn_{21-0.5x}Co_{21-0.5x}$ with x=6, 10, 14, and 22) and corrosion behavior. The HEAs were successfully designed, synthesized and confirmed to possess a single-phase FCC structure. Preliminary electrochemical corrosion characterization was conducted to gain fundamental understanding of the effects of HEA composition on corrosion resistance, which will be utilized to develop mechanistic corrosion models that enable the optimal design of corrosion resistant HEA. Unexpected passivity has been observed in the HEA containing only 6 at.% Cr.

Key Words: High entropy alloy; corrosion; CALPHAD; phase diagram; modeling

[1] Corresponding author.
E-mail address: plu@questek.com (P. Lu).

Graphical Abstract

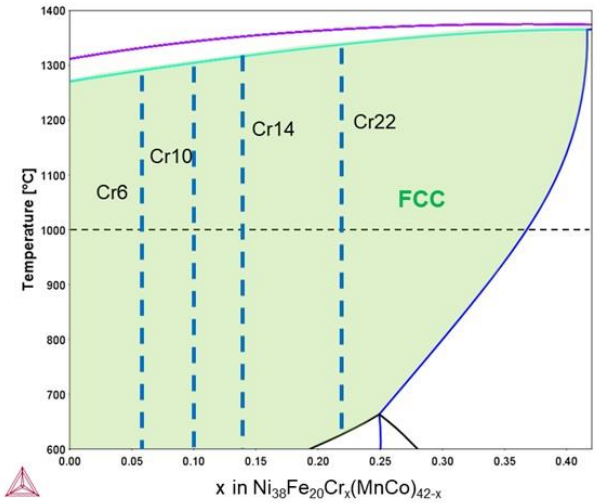

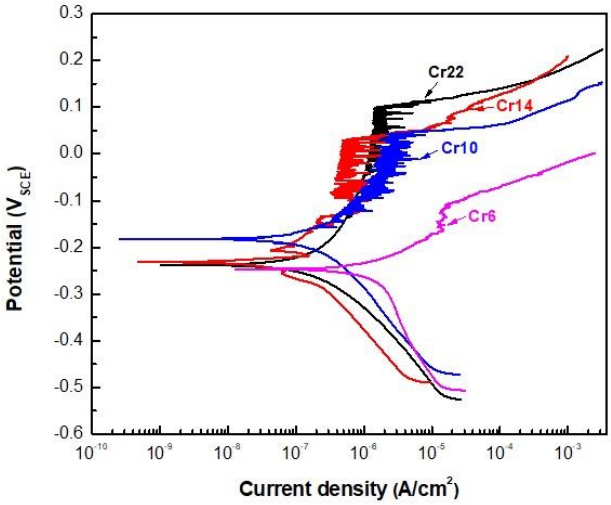

Corrosion has been identified as a major obstacle to achieving many engineering grand challenges and to implementing novel products and technologies, according to a recent national academy study [1]. To meet the stringent demands for high durability in future applications, there is a pressing need for new corrosion resistant alloys (CRAs) that have superior intrinsic corrosion resistance and are able to withstand harsh service environments. High entropy alloys (HEAs) are an emerging class of materials that have exhibited promising characteristics to achieve this objective. HEAs are complex alloys made of five or more elements at or near equimolar composition [2, 3]. They are distinct from conventional alloys since they are comprised of multiple principal elements rather than one single host element such as Fe in steels and Ni in superalloys, with major and minor alloying additions in limited concentration. Thus, HEAs remove compositional constraints seen in conventional alloy design and open up a considerable design space, with many degrees of freedom and opportunities for optimizing alloy composition and, consequently, properties. Numerous HEA systems with potentially high corrosion resistance have been investigated [4-16]. While most of the published studies focus on equimolar or simple substitutional derivatives of equimolar HEA compositions, it is worth noting that the corrosion performance of HEAs is generally not optimized for such configurations, given the strong dependence of corrosion resistance on alloy composition, microstructure, and surface oxide film chemistry [17, 18]. Accordingly, motivated by the prospect of designing HEAs with optimal corrosion resistance for harsh conditions, recent efforts have been made to deviate from simple equimolar compositions and explore the vast, non-equimolar design space to identify optimal corrosion resistant HEAs (CR-HEAs) [15, 16, 19].

The paucity of corrosion studies on complex non-equimolar HEAs is partly due to the limitations of the conventional, incremental, empirical approach to CRA design, which simply is not able to address the myriad possibilities in the multi-dimensional HEA composition space. As detailed in prior publications [19, 20], such drawbacks can be overcome and the HEA exploratory efforts can be significantly facilitated with the aid of integrated computational materials engineering (ICME), an advanced systems-based approach to design materials that meet specific performance criteria by combining computational materials models and tools across multiple length scales [21]. ICME tools such as Calculation of Phase Diagrams (CALPHAD) and Density Functional Theory (DFT) can readily predict many useful microstructural and property features for alloys, including HEAs [22-24], provided that accurate databases exist. The ICME approach is ideally suited to efficiently and exhaustively search for and design CR-HEAs with sought-after attributes, guided by existing knowledge and empirical CRA performance metrics (e.g. pitting resistance equivalence number, PREN [25, 26]).

One non-equimolar, single-phase HEA ($Ni_{38}Cr_{21}Fe_{20}Ru_{13}Mo_6W_2$) with excellent corrosion resistance even in very aggressive environments has been previously designed and characterized [15, 16, 19]. In this work, the effect of HEA concentration was studied by designing and experimentally probing a series of new CR-HEAs with systematically varied compositions, having corrosion resistance expected to range from good to poor. The goal of this study is to gain deeper understanding of the corrosion behavior of HEAs as a function of chemical composition, keeping microstructure fixed to single-phase FCC, which is required for the development of fundamental mechanistic ICME corrosion models for quantitative prediction of corrosion resistance. The resistance of the $Ni_{38}Cr_{21}Fe_{20}Ru_{13}Mo_6W_2$ HEA to passivity breakdown and localized pitting corrosion was so strong that laboratory studies of these phenomena are not possible. This limits the ability to gain insights that are required for developing models for enabling additional CR-HEA designs resistant to various stages of corrosion. For instance, it might be of particular interest to develop highly corrosion resistant alloys despite modest additions of expensive passivating or dissolution inhibiting elements. In this work, the beneficial elements Mo and W were not included in the design to reduce the corrosion resistance, as well as cost. Furthermore, Ru was also excluded because its limited supply and high cost makes it impractical as an alloying addition. Four alloys containing different concentrations of Ni, Fe, Cr, Mn, and Co were considered in design. The element Cr, which is known to strongly increase aqueous corrosion resistance, was incrementally replaced with Mn and Co, which are known to be much less beneficial as passive film promoters. Single-phase HEAs remain the focus of this study because the development of homogeneous solid solution alloys with minimization of structural and chemical

heterogeneities is the best strategy for CRA design with the greatest chance for superior corrosion resistance [20]. Details of the design process, which was based on a CALPHAD approach, can be found in a previous work [19]. In brief, CALPHAD was used to identify a composition range containing the desired elements that (1) maximized the range of single-phase HEA stability and (2) exhibited a sufficiently large solutionizing temperature window to facilitate processability. The resulting design was $Ni_{38}Fe_{20}Cr_x(MnCo)_{42-x}$, where Cr decreased from 22% and Mn and Co increased, maintaining Mn:Co=1:1, or alternatively $Ni_{38}Fe_{20}Cr_xMn_{21-0.5x}Co_{21-0.5x}$.

To summarize the designed HEA composition space, a pseudo-binary phase diagram is shown in Figure 1, where Cr content is varied and balanced by (Mn+Co). This diagram shows the amount of (Mn+Co) that can be substituted by Cr at different temperatures while still retaining a stable single FCC phase. It can be observed that this particular HEA composition space has a large single phase region that spans from 0% to as much as 40% Cr, over temperatures from 600 ~ 1200 °C. This indicates that good processability can be achieved by simple solutionization and quenching treatments. As shown in Figure 1, four HEA compositions with widely different levels of Cr content (6 at.%, 10 at.%, 14 at.%, and 22 at.%) have been selected. The compositions are reported in Table 1, and are notated as Cr6, Cr10, Cr14, and Cr22, respectively. These HEA designs are predicted to be single-phase, amenable to processing, and expected to have greatly varied corrosion behavior due to the difference in Cr content, which is suitable for studying and subsequently modeling the effect of HEA composition on corrosion performance.

For experimental evaluation of their corrosion behavior, the newly designed HEAs were prepared by arc melting of pure elements (> 99 % trace metals basis) under a pressurized argon atmosphere of 0.5 atm. The elements were arranged in ascending order of their melting point from bottom to top of the crucible. An extra 1 wt.% of Mn was added to the initial materials to compensate for the expected evaporation of Mn, which occurs during arc melting of Mn-rich alloys [27]. The arc melting chamber was purged with argon and held under vacuum, and then the elements were melted. Additionally, to improve homogeneity, each sample was flipped and melted at least five times. Buttons of all four alloy compositions of about 1 cm thickness and 2 cm in diameter were made. Prior to heat treatment, they were vacuum encapsulated and backfilled to 0.125 atm of Ar gas. To obtain single-phase FCC alloys with uniformly distributed compositions, these buttons were heat treated at 1100°C (based on Figure 1) for 96 hours followed by water quenching. The alloys were polished to a 1µm finish using diamond paste and cleaned with ethanol before microstructural characterization. Microstructure and composition of these alloys were characterized by X-ray diffractometry (XRD) and a scanning electron microscope (SEM) equipped with energy dispersive spectroscopy (EDS).

All four homogenized samples appear to be single phase in the SEM/EDS with no inclusions or segregation of alloying elements. The chemical composition distribution of Ni, Fe, Cr, Mn, and Co are uniform as shown in the EDS maps of solutionized Cr22 in Figure 2(a). Cr14, Cr10, and Cr6 also displayed a uniform chemical composition with respect to each alloying element. Figure 2(b) shows the XRD patterns of the four HEAs after homogenization, with all four alloys exhibiting single FCC crystalline structures. Well-defined diffraction peaks can be observed for the alloys with higher Cr content whereas the diffraction peaks of the low Cr alloys are noisier. The FCC structure indicates that the CALPHAD predictions were accurate, and that the structure was not altered by the water quenching from 1100°C. Thus, the ICME approach using CALPHAD was successful in predicting the structure of these alloys, similar to what was shown previously for $Ni_{38}Cr_{21}Fe_{20}Ru_{13}Mo_6W_2$ [19].

Preliminary electrochemical characterization on the four HEAs was also conducted. For polarization testing, the samples were connected to a wire, mechanically ground with SiC paper to 1200 grit, wrapped with polytetrafluoroethylene (PTFE) tape and coated with black wax, leaving an exposed working area of 0.2 ~ 0.3 cm^2 for testing. The polarization tests were conducted in a standard jacketed three electrode cell connected to a temperate controlled circulator, which maintained the temperature at 30°C. The solution was air-exposed 0.6 M NaCl solution prepared from deionized water and analytical grade NaCl. The conventional three-electrode cell setup was used, consisting of the samples as working electrode, a platinum

sheet as counter electrode, and a saturated calomel reference electrode (SCE). A Gamry Reference 600 potentiostat was used to control the potential. Prior to the experiment, the open circuit potential (OCP) was measured for 10 min, cathodically polarized at -1 V_{SCE} for 3 min in an attempt to reduce the air-formed oxide, and then kept at the OCP for 10 min to reach a stable condition. The potential was then scanned at a rate of 20 mV min^{-1} from -0.25 V versus OCP to the potential where the anodic current reached 1 mA. Following the polarization experiments, the black wax was removed, and the samples were washed and then dried with compressed air. Thereafter, the morphology of the corroded surface was examined by SEM. In addition to polarization, potentiostatic electrochemical impedance spectroscopy (EIS) was performed. The testing solution was 0.6 M NaCl that was deaerated with N_2 gas before and during testing. Prior to EIS measurements, each sample was held at the OCP for 10 min and then EIS testing was conducted at the OCP with a 20 mVrms AC signal swept over a frequency range from 10^5 to 10^{-3} Hz.

Figure 3(a) displays typical potentiodynamic polarization curves (potential vs. log[current density]) of the alloys in 0.6 M NaCl at 30°C. All four alloys exhibited passivity and breakdown as indicated by a sudden increase in current. The passive current densities are comparable for Cr10, Cr14 and Cr22, whereas that for Cr6 is significantly higher. Nonetheless, this alloy with only 6 at.% Cr was passive at OCP and exhibited breakdown at applied more positive anodic potentials. Figure 3(a) also shows the presence of many current transients in the passive region in all the alloys, at potentials slightly higher than their respective OCPs, and well below their breakdown potentials. These current transients are indicative of numerous metastable pitting events. The comparatively smaller amount of noise in the curve for Cr6 is the result of the much higher background passive current density, but it is likely that the noise in that curve was still the result of metastable pits. The frequent breakdown and repassivation events in the passive region indicates that the passive films formed on these alloys were susceptible to Cl^- induced instabilities. Examination of the sample surfaces after each test proved that the stable breakdown events associated with the persistent increases in current were crevice corrosion along the edge of the exposed area, as shown in Figure 3(b). Large pits were never observed on masked samples tested by immersion in a cell, showing that these alloys are highly susceptible to crevice corrosion and the potentials corresponding to sharp current density increase are crevice corrosion potential, E_{crev}. Thus, as shown in Figure 3(a), the crevice potential nominally increases with increasing Cr content, an expected observation due to the beneficial effect of Cr on hindering Cl^- induced passivity breakdown. Measurements of pitting potentials in the absence of crevice corrosion will be presented in a subsequent publication.

The EIS results

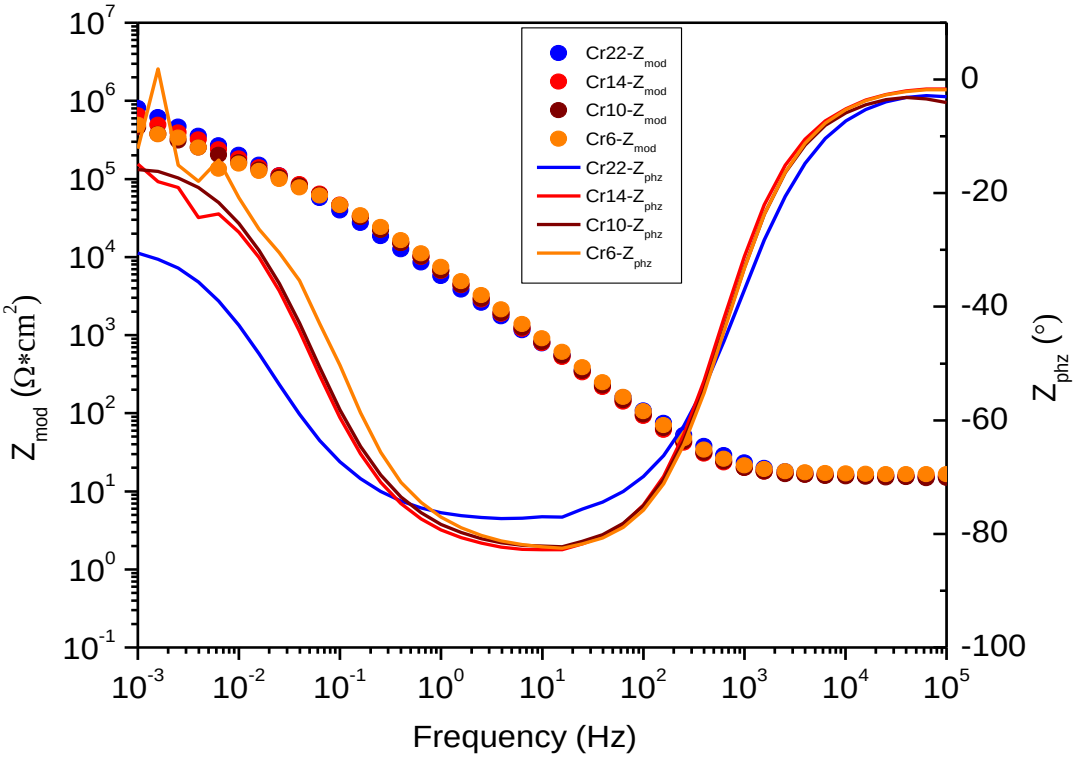

(

Figure 4) indicate very high impedance at all Cr contents, suggestive of a spontaneous passive film formed at the OCP values, which were well below E_{crev}. The impedance modulus was a weak function of Cr content with a slight decrease from 20 at.% to 6 at.% Cr. The polarization resistance obtained at the low frequency limit was above 5×10^5 Ω-cm^2, consistent with a passive dissolution rate. Notably, the alloy with 6 at.% Cr exhibits passivity at OCP despite a Cr content below typical thresholds required for passivation in binary Ni-Cr and Fe-Cr alloys [28, 29]. A subsequent publication will explore this preliminary finding in greater detail.

In summary, the ICME approach has been employed again in this work to design a series of single-phase, processable CR-HEAs with systematically varied compositions and corrosion behavior. Compared to the prior HEA, which contained Mo, W and Ru, compositional modifications were made to maintain a single phase FCC structure but lower the corrosion resistance of alloys to a level amenable to assessment of localized corrosion susceptibility using common laboratory testing techniques. The four new non-equimolar HEA compositions, $Ni_{38}Fe_{20}Cr_{22}Mn_{10}Co_{10}$, $Ni_{38}Fe_{20}Cr_{14}Mn_{14}Co_{14}$, $Ni_{38}Fe_{20}Cr_{10}Mn_{16}Co_{16}$, and $Ni_{38}Fe_{20}Cr_{6}Mn_{18}Co_{18}$, have homogenous single-phase microstructure after solutionization as predicted by CALPHAD and exhibit the expected corrosion behavior trend with changing Cr content. However, $Ni_{38}Fe_{20}Cr_{6}Mn_{18}Co_{18}$, which contains only 6 at.% Cr and 38 at.% Ni, showed surprisingly good passivity. This could result from some unidentified positive synergy between Cr and other elements that promotes partitioning of Cr to surfaces and passive film formation.

ACKNOWLEDGEMENTS

This work was supported as part of the Center for Performance and Design of Nuclear Waste Forms and Containers, an Energy Frontier Research Center funded by the U.S. Department of Energy, Office of Science, Basic Energy Sciences under Award # DE-SC0016584.

REFERENCES

[1] NAS Grand Challenges for Engineering, National Academy Press, 2008.
[2] J.W. Yeh, S.K. Chen, S.J. Lin, J.Y. Gan, T.S. Chin, T.T. Shun, C.H. Tsau, S.Y. Chang, Adv. Eng. Mater. 6 (2004) 299-303.
[3] M.H. Tsai, J.W. Yeh, Mater. Res. Lett. 2 (2014) 107-123.
[4] C.P. Lee, C.C. Chang, Y.Y. Chen, J.W. Yeh, H.C. Shih, Corros. Sci. 50 (2008) 2053-2060.
[5] Y.L. Chou, J.W. Yeh, H.C. Shih, Corros. Sci. 52 (2010) 2571-2581.
[6] Z. Liu, J.M. Zeng, H.H. Zhan, Appl. Mech. Mater. 117-119 (2012) 1816-1819.
[7] B. Ren, Z.X. Liu, D.M. Li, L. Shi, B. Cai, M.X. Wang, Mater. Corros. 63 (2012) 828-834.
[8] X.W. Qiu, Y.P. Zhang, L. He, C.G. Liu, J. Alloy. Compd. 549 (2013) 195-199.
[9] Y. Qiu, M. Gibson, H. Fraser, N. Birbilis, Mater. Sci. Tech-Lond. 31 (2015) 1235-1243.
[10] V. Soare, D. Mitrica, I. Constantin, G. Popescu, I. Csaki, M. Tarcolea, I. Carcea, Metall. Mater. Trans A. 46A (2015) 1468-1473.
[11] Z. Zhang, E. Axinte, W. Ge, C. Shang, Y. Wang, Mater. Des. 108 (2016) 106-113.
[12] D.B. Miracle, O.N. Senkov, Acta Mater. 122 (2017) 448-511.
[13] Y. Qiu, S. Thomas, M.A. Gibson, H.L. Fraser, N. Birbilis, npj Mater. Deg. 1 (2017) 15.
[14] Y. Qiu, S. Thomas, M. Gibson, H. Fraser, K. Pohl, N. Birbilis, Corros. Sci. (2018) 386-396.
[15] T. Li, O.J. Swanson, G.S. Frankel, A.Y. Gerard, P. Lu, J.E. Saal, J. R. Scully, Electrochim. Acta. 306 (2019) 71-84.
[16] K.F. Quiambao, S.J. McDonnell, D.K. Schreiber, A.Y. Gerard, K.M. Freedy, P. Lu, J.E. Saal, G.S. Frankel, J.R. Scully, Acta Mater. 164 (2019) 362-376.
[17] C. Lee, Y. Chen, C. Hsu, J. Yeh, H. Shih, Thin Solid Films. 517 (2008) 1301-1305.
[18] Q. Li, T. Yue, Z. Guo, X. Lin, Metall. Mater. Trans A. 44 (2013) 1767-1778.
[19] P. Lu, J.E. Saal, G.B. Olson, T. Li, O.J. Swanson, G.S. Frankel, A.Y. Gerard, K.F. Quiambao, J.R. Scully, Scripta Mater. 153 (2018) 19-22.
[20] C.D. Taylor, P. Lu, J. Saal, G.S. Frankel, J.R. Scully, npj Mater. Deg. 2 (2018) 6.
[21] C. Kuehmann, G. Olson, Mater. Sci. Tech-Lond. 25 (2009) 472-478.
[22] C. Zhang, M.C. Gao, CALPHAD modeling of high-entropy alloys, in: High-Entropy Alloys, Springer, 2016, pp. 399-444.
[23] C. Niu, A. Zaddach, C. Koch, D. Irving, J. Alloy. Compd. 672 (2016) 510-520.
[24] J.E. Saal, I.S. Berglund, J.T. Sebastian, P.K. Liaw, G.B. Olson, Scripta Mater. 146 (2018) 5-8.
[25] N. Dowling, Y.-H. Kim, S.-K. Ahn, Y.-D. Lee, Corros. 55 (1999) 187-199.
[26] G. Herbsleb, Materials and Corros. 33 (1982) 334-340.
[27] F. Otto, Y. Yang, H. Bei, E.P. George, Acta Mater. 61 (2013) 2628-2638.
[28] E. McCafferty, J. Electrochem. Soc. 150 (2003) B238-B247.
[29] E. McCafferty, Corros. Sci. 47 (2005) 1765-1777.

Table 1: Chemical compositions of the high entropy alloys (at.%) within the $Ni_{38}Fe_{20}Cr_xMn_{21-0.5x}Co_{21-0.5x}$ compositional space that are predicted to be single-phase with large solutionizing temperature window by CALPHAD in Thermo-Calc software using TCHEA3 database.

Designation	Ni	Fe	Cr	Mn	Co
Cr22	38	20	22	10	10
Cr14	38	20	14	14	14
Cr10	38	20	10	16	16
Cr6	38	20	6	18	18

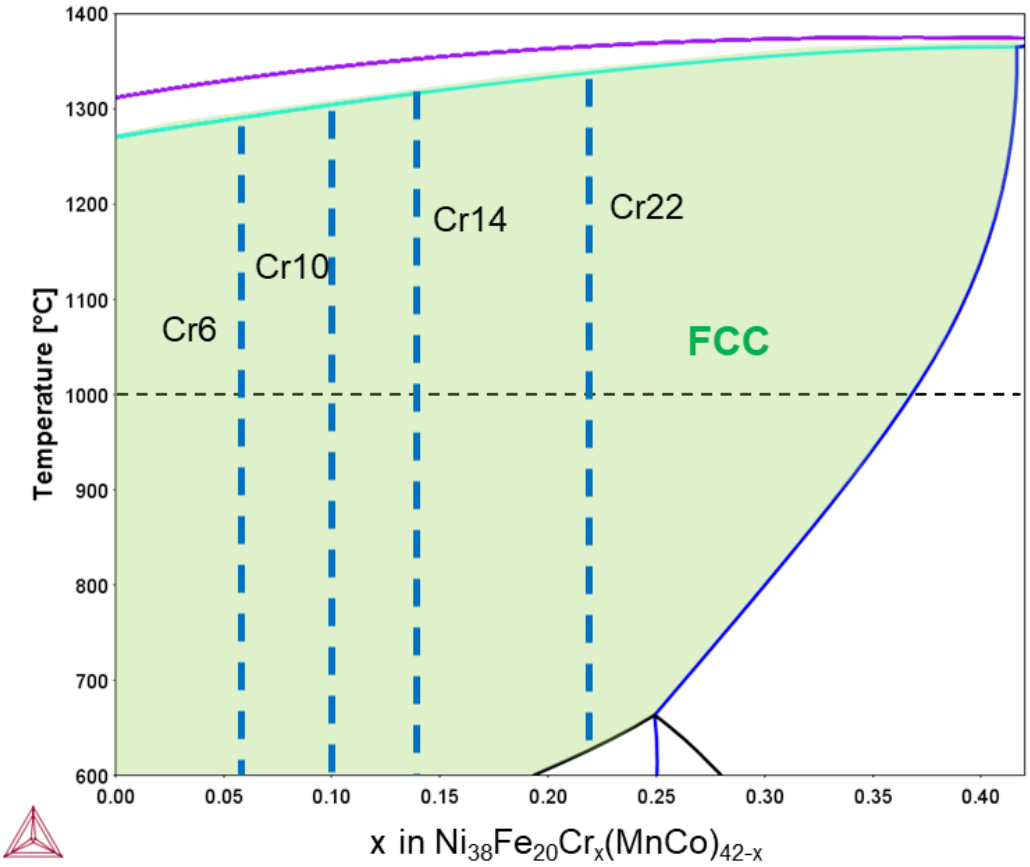

Figure 1. Pseudo-binary phase diagram of $Ni_{38}Fe_{20}Cr_x(MnCo)_{42-x}$ with Mn:Co=1:1 calculated in Thermo-Calc with TCHEA3 database. The FCC single phase region is shaded in green.

(a)

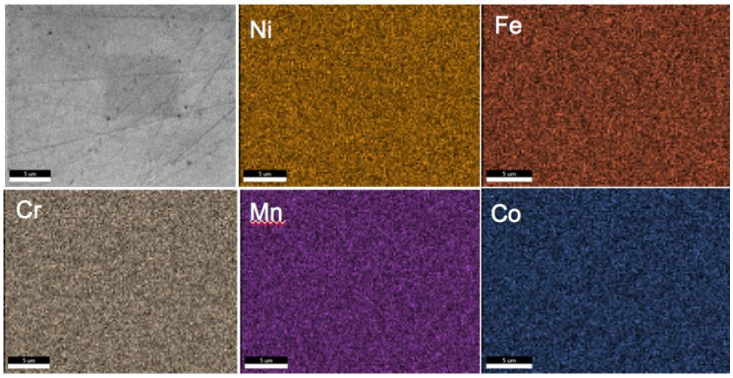

(b)

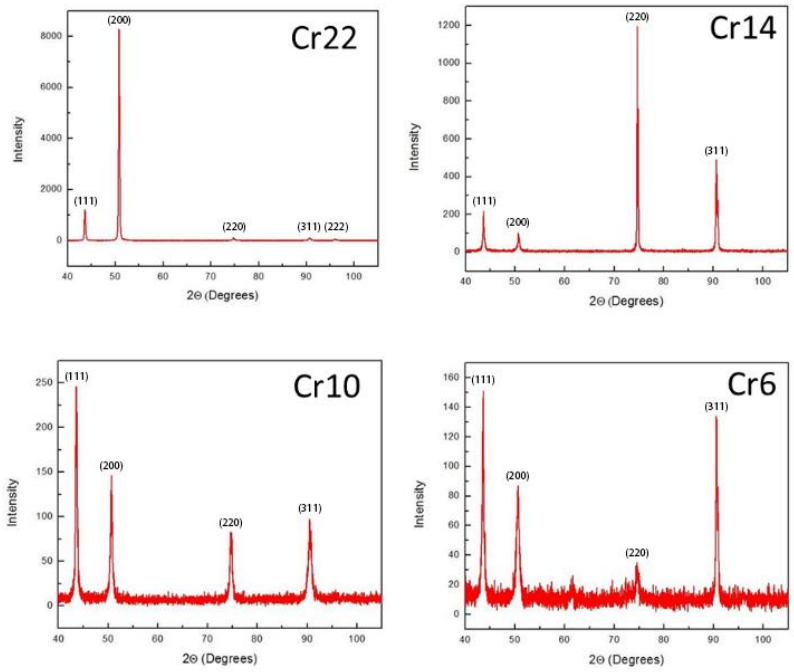

Figure 2: (a) EDS mapping of Cr22 after homogenization at 1100ºC for 96 hours, displaying uniform distribution of elements. (b) XRD patterns of Cr22, Cr14, Cr10, and Cr6 with peaks corresponding to FCC structure.

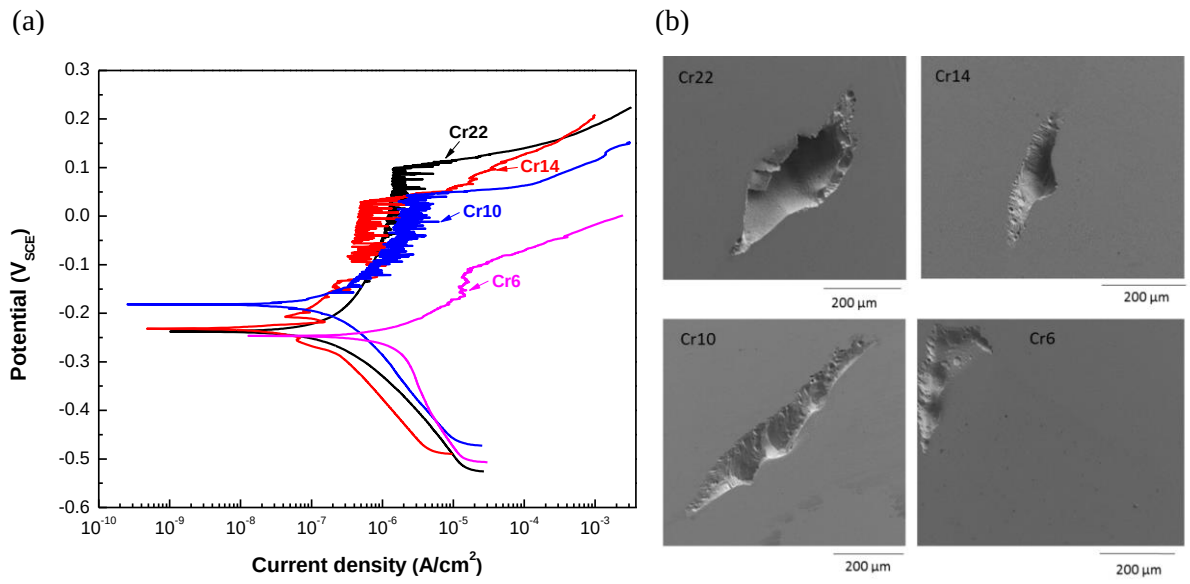

Figure 3: (a) Potentiodynamic polarization curves of the HEAs in 0.6 M NaCl solution at 30°C in an air-exposed immersion cell; (b) SEM images of crevice corrosion along the edge of the exposed area found after polarization in 0.6 M NaCl at 30°C in an air-exposed immersion cell.

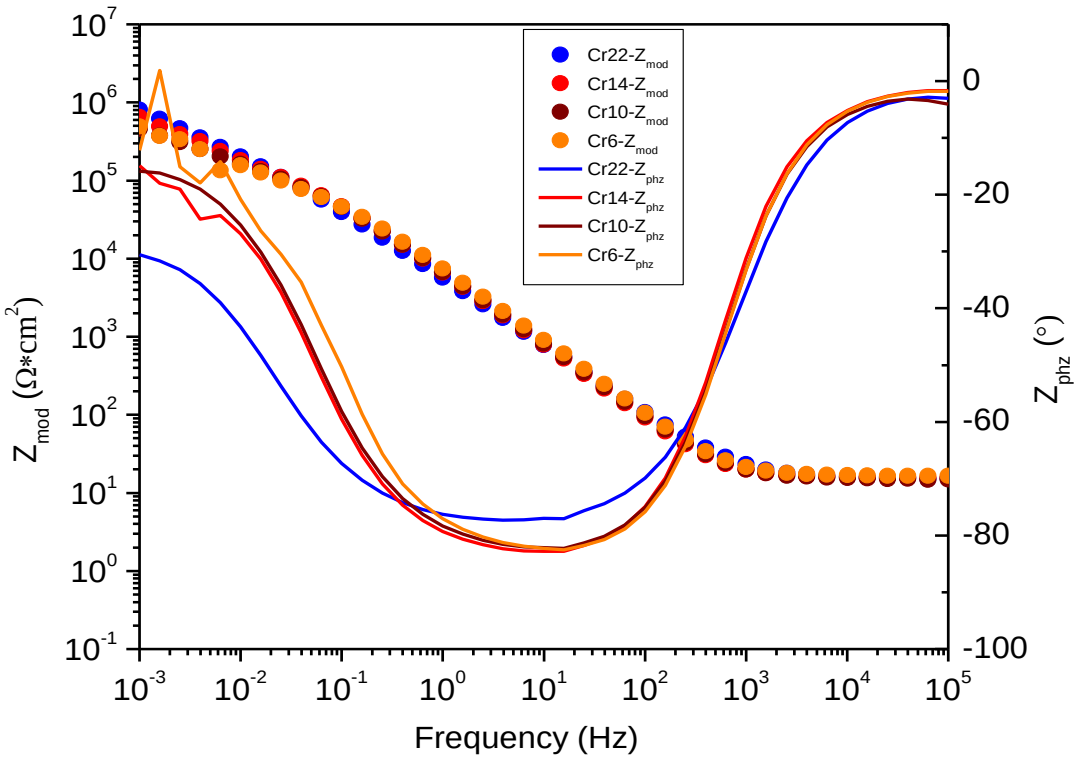

Figure 4: EIS results showing the impedance modulus, Z_{mod}, and phase angle, Z_{phz}, for HEA Cr6, Cr10, Cr14, and Cr22 after a 10 min OCP hold in N_2-deaerated 0.6M NaCl solution at ambient temperature.